remote sensing

MDPI

Article

Impacts of Quasi-Biennial Oscillation and El Niño–Southern Oscillation on Stratospheric Isentropic Mixing Process

Jing Liang, Zhiting Wang *, Zhiyi Zhang and Jiali Luo

College of Atmospheric Sciences, Lanzhou University, Lanzhou 730000, China; liangj2020@lzu.edu.cn (Jing Liang)
* Correspondence: wangzt@lzu.edu.cn

Abstract: The present study investigates the influences of stratospheric quasi-biennial oscillation (QBO) and El Niño–Southern Oscillation (ENSO) on the intensity of stratospheric isentropic mixing based on ERA-Interim and MERRA-2 reanalysis products. It is found that isentropic mixing in the stratosphere is modulated by QBO and ENSO. An analysis of the QBO basis function in the multiple regression model reveals that isentropic mixing in the lower stratosphere is suppressed in the equatorial region in the WQBO phase, while the mixing enhances in the subtropical and mid-latitude regions. This result is not consistent with the Holton–Tan mechanism. However, isentropic mixing in the mid-latitudes becomes stronger in the middle stratosphere in the EQBO phase, which agrees well with the Holton–Tan effect. Composite analysis indicates that QBO-induced changes in the direction and speed of the stratospheric zonal wind can affect wave propagation and wave breaking. In the WQBO phase, zonal wind weakens, and a planetary wave is anomalously converging near 30°N, which leads to an increase in isentropic mixing; on the contrary, wind speed becomes large, and the upward propagation of planetary wave divergence, which lead to the isentropic mixing, becomes weak near 60°N. In the EQBO phase, the wind is relatively weak around 60°N, and the isentropic mixing is strong. Multiple regression analysis reveals the ENSO impact on the intensity of isentropic mixing, which shows weak mixing in the middle and high latitudes and strong mixing in the low latitudes of the lower stratosphere in the El Niño years. In the middle stratosphere, isentropic mixing enhances in the mid-latitude region due to intensified upward propagation of planetary waves but weakens in the polar region. Composite analysis reveals a clear relationship between the mixing strength zones of the El Niño and La Niña years with the position of the polar jet and changes in zonal wind speed.

Keywords: stratospheric isentropic mixing; equivalent length; QBO; ENSO; multiple regression

Citation: Liang, J.; Wang, Z.; Zhang, Z.; Luo, J. Impacts of Quasi-Biennial Oscillation and El Niño–Southern Oscillation on Stratospheric Isentropic Mixing Process. *Remote Sens.* **2023**, *15*, 2715. https://doi.org/10.3390/rs15112715

Academic Editor: Gad Levy

Received: 4 April 2023
Revised: 17 May 2023
Accepted: 20 May 2023
Published: 23 May 2023

1. Introduction

Isentropic mixing in the stratosphere is an important component of global mass transport, which has significant impacts on mass transport and composition distribution in the stratosphere. Isentropic mixing and diabatic transport (updrafts in the tropics, downdrafts in wave breaking zones) play an important role in stratospheric transport. Stratospheric mixing mainly occurs along isentropic surfaces (quasi-horizontal), leading to a smaller meridional gradient of long-lived trace gases. The slow diabatic overturning circulation, by contrast, results in a continuous increase in the meridional gradient of long-lived trace gases [1,2].

Many diagnostic methods have been proposed for the study of isentropic mixing in the stratosphere. The mixing on the isentropic surface can be diagnosed based on potential vorticity (PV), which is conserved in the absence of friction and diabatic heating. Therefore, PV isolines can be taken as isolines of air–mass tracers. This approach has been applied to reveal the transport boundary of meridional mixing [3]. Another approach is to describe the mixing properties in the stratosphere by calculating the effective diffusion coefficient [4]. The effective diffusion coefficient is a modified Lagrangian mean diagnostic quantity, which simplifies the two-dimensional tracer advection–diffusion equation into a one-dimensional diffusion equation by introducing a tracer mixing ratio-based coordinate. A large diffusion coefficient corresponds to strong mixing, and a small one corresponds to weak mixing, which can be used to identify the transport boundary. This diagnostic approach is an effective way to identify a transport boundary and regions of strong mixing (wave breaking regions) [5–7].

The mixing and transport process in the stratosphere is closely related to wave activities. There exist waves of various scales in the middle and upper atmosphere, such as planetary waves, tides, and gravity waves. These waves break up when they reach a critical condition or become incapable of propagating, and the energy and momentum carried by the waves are then dissipated into the background atmosphere. In the stratosphere, tracer distribution is affected by residual circulation and isentropic mixing caused by wave breaking (e.g., planetary wave breaking) [8]. Given the close relationship between mixing and Rossby wave activities, the mixing properties in the stratosphere are affected by strong interannual variability of planetary waves. The stratospheric quasi-biennial oscillation (QBO) and the El Niño–Southern Oscillation (ENSO) are two major climate variability signals in the tropics, and they are also the main climate factors affecting stratospheric circulation and mixing. Existing studies have found that QBO and ENSO have very important impacts on planetary wave breaking [9–14]. QBO will affect wave propagation by adjusting the position of zero wind speed line and the width of the waveguide. Meanwhile, changes in zonal winds will cause the movement of the wave breaking position and, subsequently, affect isentropic mixing in the stratosphere [15,16]. ENSO can affect stratospheric circulation and isentropic mixing by modulating anomalous propagation and breaking of ultra-long stratospheric Rossby waves [17–19].

The QBO impact on regions outside the tropics is called the Holton–Tan effect; that is, when the equatorial QBO is in the westerly phase (WQBO), the planetary waves in the stratosphere propagate more equatorward, and the polar vortex in the Arctic becomes stronger and more stable; when the equatorial QBO is in the easterly phase (EQBO), the planetary waves in the stratosphere propagate more poleward [20]. Note that in addition to changing the position of the zero-wind line, the acceleration/deceleration of the tropical zonal mean wind associated with the QBO can also cause anomalous overturning circulation, which can extend to the subtropical region and lead to further zonal mean wind anomalies and temperature anomalies [21]. White et al. [22] found that during the QBO easterly phase, the upward propagation of planetary waves from the troposphere to the stratosphere increases, which is attributed to the joint effects of wave aggregation in high latitudes induced by the positional change in the zero-wind line and the meridional circulation in the subtropics associated with the QBO. Moreover, the QBO signal appears in the extratropics mainly because of the modulation of propagation background for the waveguide from the troposphere to the stratosphere rather than the modulation of the tropospheric wave source [23].

During most of the El Niño episodes, anomalous upward propagation and the breaking of planetary waves in the mid- and high-latitude regions enhance the BD circulation and the mixing in the stratosphere [11,24–26]. In their studies of how ENSO impacts the polar stratosphere in the Northern Hemisphere, Van Loon et al. [27] and Van Loon and Labitzke [28] tried to distinguish the influences of QBO and ENSO. However, the study of Hamilton [29] indicates that the signals of ENSO and QBO statistically are indistinguishable. Papers discussing observational evidence also point out that the QBO impacts actually mask most of the ENSO impacts. Most studies mainly discuss the seasonal variation of stratospheric mixing and regulation mechanisms of QBO and ENSO on the stratospheric polar vortex. It is found that the zero wind speed line in the Holton–Tan mechanism and the mean meridional circulation associated with the QBO zonal wind play an important role in the response of polar stratosphere. More planetary waves are reflected back to mid- and high latitudes in the QBO easterly phase. ENSO can modulate the intensity of the polar vortex, and the anomalous upward propagation and breaking of planetary waves in high latitudes in the El Niño years lead to a weakened stratospheric polar vortex [30–35].

Changes in the intensity of stratospheric isentropic mixing are also related to QBO and ENSO. Studying the influences of QBO and ENSO on mixing intensity can help us better understand transport processes in the stratosphere. Current research of the influences of QBO and ENSO on the mixing at different heights throughout the stratosphere are not detailed enough, and the physical mechanisms for QBO and ENSO impacts on isentropic mixing in the stratosphere needs further investigation.

In the present study, we use ERA-Interim and MERRA-2 reanalysis products to calculate the equivalent length based on potential vorticity distribution and diagnose the isentropic mixing in the stratosphere. The interannual variation of isentropic mixing intensity within the 400 K–1200 K region during 1980–2010 is studied, the influences of QBO and ENSO on the stratospheric mixing intensity are analyzed, and the mechanisms for these influences are explored.

2. Data and Methods

2.1. Data

Temperature, potential vorticity, and wind at 11 pressure levels from ERA-Interim reanalysis daily data and at 13 pressure levels from MERRA-2 reanalysis daily data within the range of 100 hPa–1 hPa for the period 1980–2010 were employed in the present study. The horizontal resolutions were 0.75° × 0.75° and 0.5° × 0.625° for ERA-Interim and MERRA-2 products, respectively. The PV on pressure levels was vertically interpolated to the isentropic surfaces of 400 K, 480 K, 560 K, 640 K, 720 K, 800 K, 880 K, 960 K, 1040 K, 1120 K, and 1200 K.

2.2. Methods

2.2.1. Calculation of the Equivalent Length

The effective diffusion coefficient is a measure of the complexity or elongation of the tracer contour caused by the horizontal wind field on the isentropic surface. The advection diffusion equation for a tracer with the concentration $c(x, t)$ can be expressed as [4]:

$$\frac{\partial c}{\partial t} + \boldsymbol{u} \cdot \nabla c = \nabla \cdot (k \nabla c) \tag{1}$$

where $\mathbf{u}$ is the horizontal wind vector and k is the constant parameter of the diffusion coefficient. By defining a coordinate based on the tracer concentration, the equivalent latitude ϕ_e, the equation (R-4) can be transformed into a pure diffusion equation:

$$\frac{\partial C}{\partial t} = \frac{1}{r^2 cos\phi_e} \frac{\partial}{\partial \phi_e} (k_{eff} cos\phi_e \frac{\partial C}{\partial \phi_e}) \tag{2}$$

$C(\phi_e,t)$ is expressed as the tracer concentration in the equivalent latitude coordinates, r is the radius of the Earth, and k_{eff} is the effective diffusivity. Based on previous studies, the effective diffusion coefficient is defined as [4,6]:

$$k_{eff} = kr^2 \frac{\langle |\nabla c|^2 \rangle}{(\partial C / \partial \phi_e)^2} \tag{3}$$

The angle brackets indicate the average of the area between the consecutive tracer lines. Given the relatively long time scale of adiabatic motion in the stratosphere, potential vorticity (PV) is usually used to diagnose the evolution of tracers on the isentropic surface since PV is conserved under an adiabatic condition [36–39]. Meanwhile, temporal evolution of the tracer contour is correlated with the intensity of wave activities, whose impact on transport can be represented by the effective diffusion coefficient [30,35]. The equivalent length L_e is defined such that

$$k_{eff}(\phi_e, t) = k \frac{L_e^2(\phi_e, t)}{(2\pi r cos\phi_e)^2} \tag{4}$$

We show the values of the normalized equivalent length squared, and the equivalent length can be defined as [30]

$$\Lambda_e = \frac{L_e^2}{(2\pi r cos\phi_e)^2} = \frac{k_{eff}}{k} \quad (5)$$

Λ_e represents the estimate of the minimum tracer contour elongation relative to its original pattern. Larger values of the equivalent length indicate regions of strong mixing where the tracer contour is greatly stretched. Meanwhile, the equivalent length is closely related to the wave activities and can increase due to wave breaking.

The value of the equivalent length depends on the model resolution. It increases monotonically as the grid scale becomes finer. Although the value of the equivalent length is resolution-dependent, major characteristics of its spatiotemporal distribution are largely resolution-independent. Therefore, barriers to the mixing and strong mixing regions can be identified by the minimum and maximum values of the equivalent length.

2.2.2. Multiple Linear Regression Model

In order to distinguish the impacts of QBO and ENSO on wave activities from sources of other natural variability, this study employed a multiple regression model to analyze temporal evolution of the monthly zonal mean equivalent length. Details of this method and its application can be found in Diallo et al. [40–42].

$$\chi(t,\phi,z) = a(\phi,z)\cdot t + C(t,\phi,z) + \sum_{k=1}^{2} b_k(\phi,z)\cdot P_k(t - \tau_k(\phi,z)) + \epsilon(t,\phi,z) \quad (6)$$

$$C(t,\phi,z) = a_0(\phi,z) + \sum_{k=1}^{4} [a_{ks}(\phi,z) sin(2\pi k(t-0.5)/12) + a_{kc}(\phi,z) cos(2\pi k(t-0.5)/12)] \quad (7)$$

ϕ is the equivalent latitude, z represents the height of the isentropic surface in the stratosphere, P_k denotes various explanatory variables, and P_1 is the QBO index (QBOi), which is derived from the normalized 50 hPa zonal mean wind speed of the CDAS/reanalysis data. P_2 is the normalized multivariate ENSO index (MEI) [43]. The coefficient is the linear trend a, $C(t,\phi,z)$ is the annual cycle, b_1 is the amplitude, and lag τ_1 is the lag related to QBO. b_2 is the amplitude, d τ_2 is the lag related to ENSO, and $\epsilon(t,\phi,z)$ is the residual.

2.2.3. Eliassen–Palm Flux

The E–P flux is the wave action flux in the spherical atmosphere and can be used to characterize the propagation of planetary waves. It is also a useful tool for diagnosing wave-flow interactions. In the spherical pressure p-coordinate system and quasi-geostrophic approximation, the E–P flux vector (the unit is m^2/s^2) can be calculated by [44,45]:

$$\boldsymbol{F} = \{F_{(\varphi)}, F_{(p)}\} = \left\{ -r_0 cos\varphi\overline{u'v'}, \frac{f r_0 cos\varphi\overline{v'\theta'}}{\overline{\theta}_p} \right\} \quad (8)$$

The dispersion of E–P fluxes (the unit is m/(s·d)) can be calculated by:

$$\nabla\cdot\boldsymbol{F} = \frac{1}{\boldsymbol{r_0 cos\varphi}} \frac{\partial}{\partial\varphi}\left(F_{(\varphi)} cos\varphi\right) + \frac{\partial}{\partial p}\left(F_{(p)}\right) \quad (9)$$

where $F_{(\varphi)}$,$F_{(p)}$ denote fluctuation effects, vortex angular momentum transport (magnitude of 10^8 m^3/s^2), and vortex heat transport per unit mass of air in the north–south direction (magnitude is 10^6 $Pa\cdot m^2/s^2$), respectively. In Equation (R-2) and Equation (R-3), r_0 is the radius of the Earth, f is the Coriolis force parameter, φ is the latitude, θ is the potential temperature, and u' and v' are the latitudinal and meridional wind disturbances, respectively. The superscripts "-" and "′" indicate the latitudinal mean and latitudinal deviation; the subscript "p" indicates the deviation from the barometric pressure.

2.2.4. Selection of MEI Index and QBO Index

The cold and warm phase years were determined using the multivariate ENSO index dataset (MEI) provided by the Earth System Research Laboratory of the National Oceanic and Atmospheric Administration of the United States (http://www.esrl.noaa.gov/psd/enso/mei/, accessed on 1 March 2023). This dataset provides bimonthly MEI values for the period 1980–2010. The ENSO composite index for winter was calculated based on the average MEI value from December/January to March/April of each year. A positive MEI value indicated the warm phase of ENSO, and an abnormally high MEI value indicated an El Niño event (MEI > 0.2). A negative MEI value indicated the cold phase of ENSO, and an abnormally low value indicated a La Niña episode (MEI < −0.2) [46–48].

Chen et al. [49] argued that 50 hPa zonal wind was most closely related to the depth of the QBO wind. In the present study, 50 hPa zonal mean wind was used to define the QBO signal; that is, when the 50 hPa zonal mean wind over 5°S–5°N in winter was greater than 3 m/s, the westerly phase of the quasi-biennial oscillation (WQBO) was identified. When the 50 hPa zonal mean wind was less than −3 m/s, the easterly phase of the quasi-biennial oscillation (EQBO) was identified. During the period 1980–2010, EQBO occurred in 9 years and WQBO occurred in 15 years.

Figure 1 displays the time series of QBO index and ENSO index at 50 hPa, respectively. Independent cases of quasi-biennial oscillation in easterly and westerly phases in Table 1 and independent ENSO events in Table 2 are selected based on the results in Figure 1. Anomalies corresponding to various events in the present study were obtained using a composite analysis based on the above two tables.

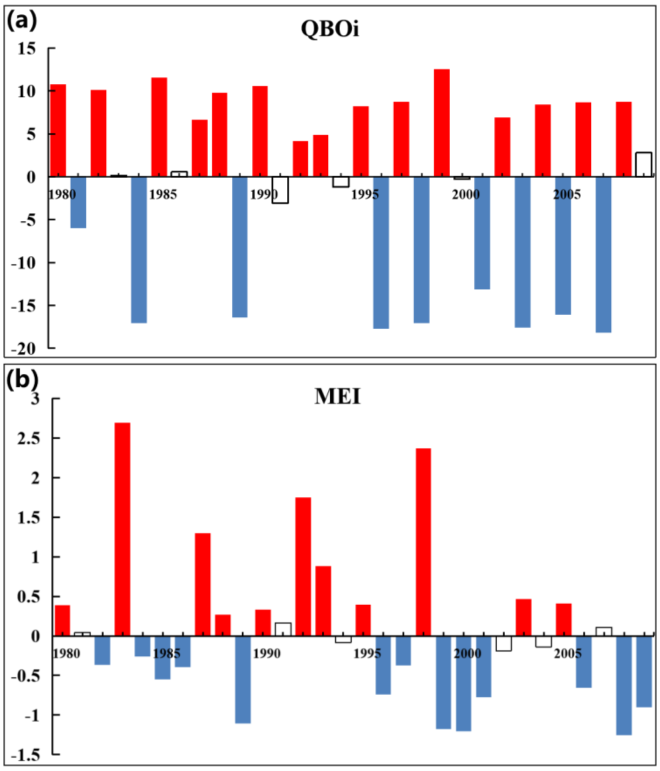

Figure 1. Time series of QBO index at 50 hPa (**a**) and MEI index (**b**) averaged in the winters from 1980 to 2010.

Table 1. EQBO and WQBO cases.

Event	Year
EQBO	1981, 1984, 1989, 1996, 1998, 2001, 2003, 2005, 2007
WQBO	1980, 1982, 1985, 1987, 1988, 1990, 1992, 1993, 1995, 1997, 1999, 2002, 2004, 2006, 2008

Table 2. El Niño and La Niña cases.

Event	Year
El Niño	1980, 1983, 1987, 1988, 1990, 1992, 1993, 1995, 1998, 2003, 2005
La Niña	1982, 1984, 1985, 1986, 1989, 1996, 1997, 1999, 2000, 2001, 2006, 2008, 2009

2.2.5. Composite Analysis

Composite analysis is often used to compare meteorological variables in different periods. Generally speaking, it is to find the average values of specific meteorological elements in different states. In the present study, we investigated four types of events, i.e., QBO westerly wind phase, QBO easterly wind phase, El Niño, and La Niña, and then we conducted a composite analysis in the years of these four types of events. To determine from the statistical perspective whether their differences are significant, we employed the *t*-test to statistically test the composite results.

3. Results and Analysis

3.1. Interannual Variability of Isentropic Mixing Intensity

In the present study, potential vorticity is used as the tracer to calculate the equivalent length at different altitudes of the stratosphere over a long time period (30 years of ERA-Interim and MERRA-2 data). We use the equivalent length Λ_e calculated from ERA-Interim data over the period 1980–2010 to analyze QBO signals in the lower (480 K) and middle stratospheric (880 K) mixing processes. The time series is de-seasonalized by calculating the monthly average of the entire time series and subtracting this value from the corresponding month to obtain the abnormal time series.

Temporal evolutions of the equivalent length at 480 K and 880 K in the tropics (30°S–30°N) are displayed in Figure 2a,b, which shows significant QBO signals in the lower stratosphere, while the QBO signals in the middle stratosphere are not obvious. Figure 2c,d displays interannual variability of isentropic mixing intensity in the Northern Hemisphere in winter. To better observe the QBO signal in the interannual variation of the equivalent length, we employed spectral analysis, such as fast Fourier transform to reveal the dominant frequencies (periods).

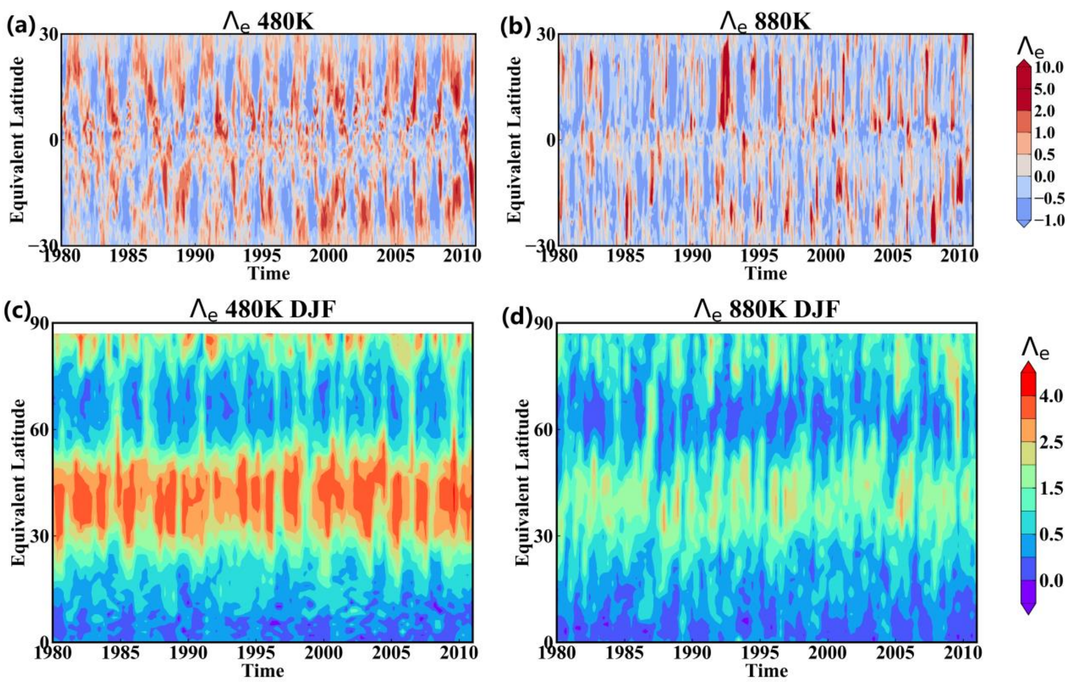

Figure 2. Interannual variabilities of the equivalent length at 480 K and 880 K in the tropics (**a**,**b**) and their winter averages (**c**,**d**) during 1980–2010 in ERA-Interim (seasonality in the data is removed).

The results of the power spectrum analysis for both data equivalent lengths are given in Figure 3. From the figure, we can see that the power spectrum of the signal with 24 to 36 monthly cycles has large value centers, and we can determine that in the QBO signal in the stratosphere.

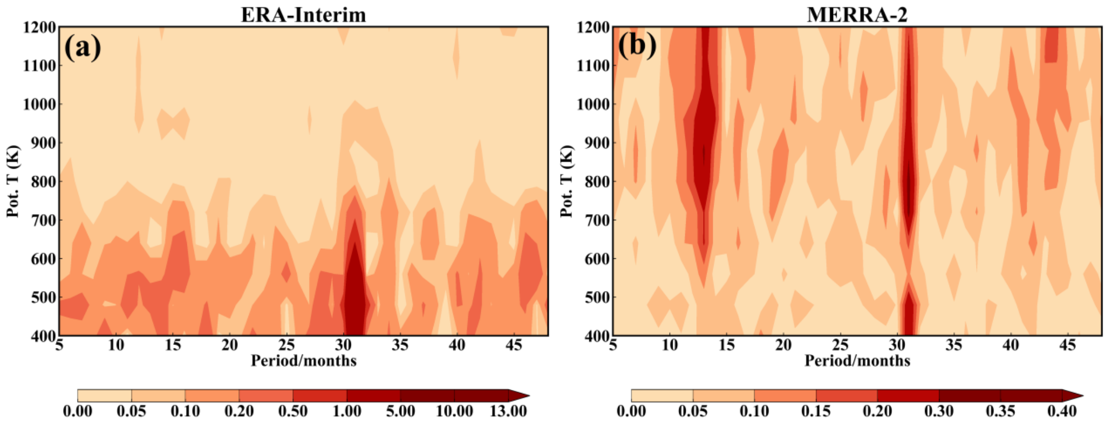

Figure 3. Frequency power spectra of the (**a**) equivalent lengths calculated from the ERA-Interim and (**b**) MERRA-2 data.

3.2. Multiple Regression Model

To explore the impacts of QBO and ENSO on isentropic mixing in the stratosphere, the relationship between QBO and ENSO is studied first. The correlation calculation (Figure 4) indicates that the correlation coefficient between QBO and ENSO during 1980–2010 is only 0.094, which cannot pass the significance test, suggesting that there is no significant correlation between QBO and ENSO.

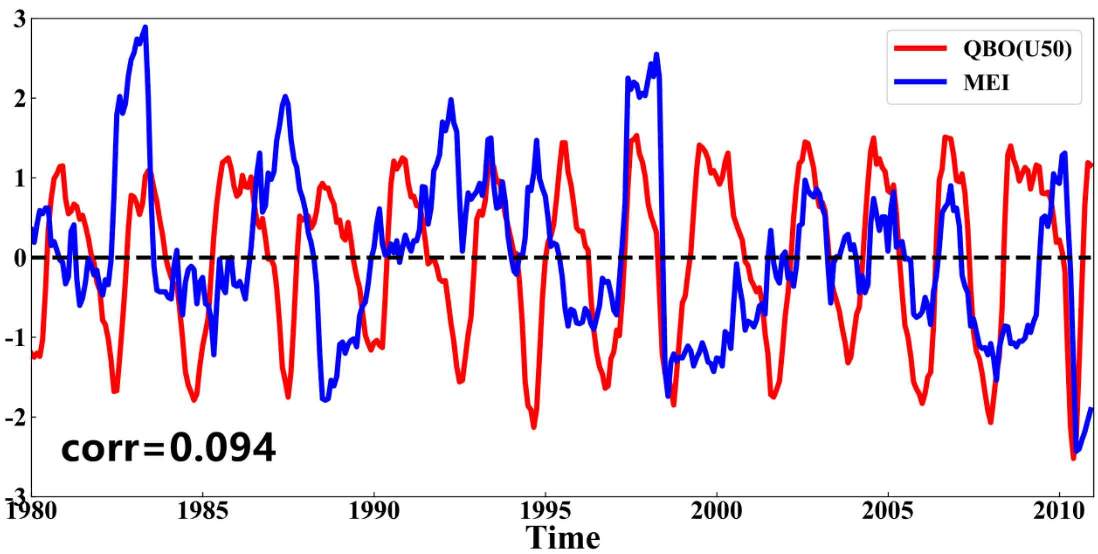

Figure 4. Sequences of the QBO index (solid red line) and MEI index (solid blue line) defined by the 50 hPa zonal mean wind in the Northern Hemisphere winter from 1980 to 2010. The vertical axis represents the value of the two indexes, and the number in the lower left corner is the correlation coefficient between the two indexes.

The multiple regression model described in Section 2 is applied to the time series of monthly zonal mean equivalent lengths at individual latitudes over the period 1980–2010. Because the fitting effect based on ERA-Interim is better, the regression model fittings based on ERA-Interim in the lower (480 K isentropic surface) and middle stratosphere (880 K isentropic surface) at three selected latitudes (low latitudes, mid-latitudes, and high latitudes of the Northern Hemisphere) are displayed in Figure 5. It shows that at the above two isentropic levels, the extreme signals in the equatorial region are obvious; especially on the 880 K isentropic surface, the annual cycle is very weak, and the regression model is hard to fit the observations. Strong annual variability appears in the mid-latitude and polar regions, and the model well fits the temporal evolution of equivalent length in these regions. For the years in which the difference between the true value and the fitted value is large, the mixing is not well represented by the regression model, indicating that some other influencing factors, such as volcanic eruptions, are not considered.

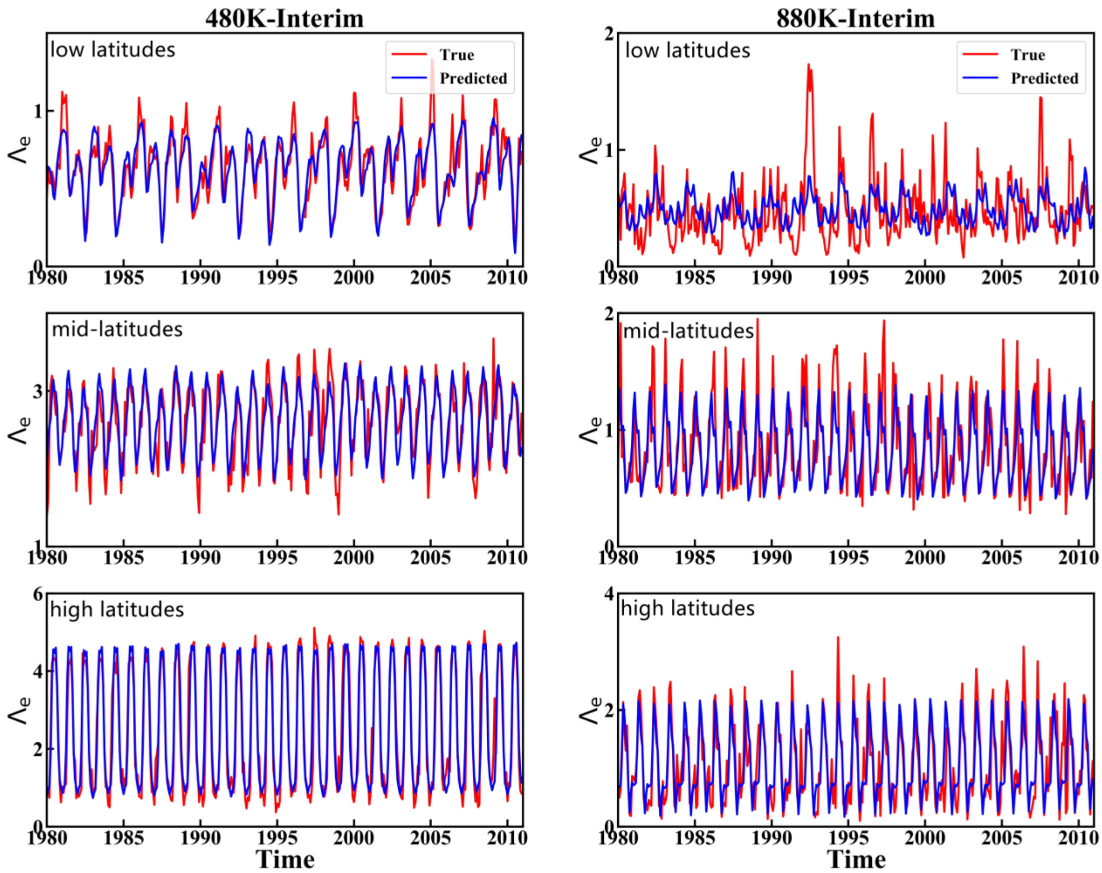

Figure 5. Time series of original value (red) and simulated value (blue) of the equivalent length calculated from ERA-Interim on the 480 K and 880 K isentropic surfaces. The two panels are regional averages for the equatorial region (0–30°N), the middle two panels are regional averages for the mid-latitude region (30–60°N), and the bottom two panels are for the polar region (60–90°N).

The $a(\phi, z)$ coefficients in Equation (R-1) are used to describe the long-term trend of the equivalent length at different levels. The contrast in the trend of equivalent length between ERA-Interim and MERRA-2 data are evident in Figure 6. Most of the regions in the ERA-Interim data from 1980 to 2010 reflect an increase in equivalent length. There is almost no difference between the two trend changes in the lower levels, while the MERRA-2 data show a weakening of the mixing in the middle and upper equatorial regions and in the upper polar regions, contrary to the results of the ERA-Interim data.

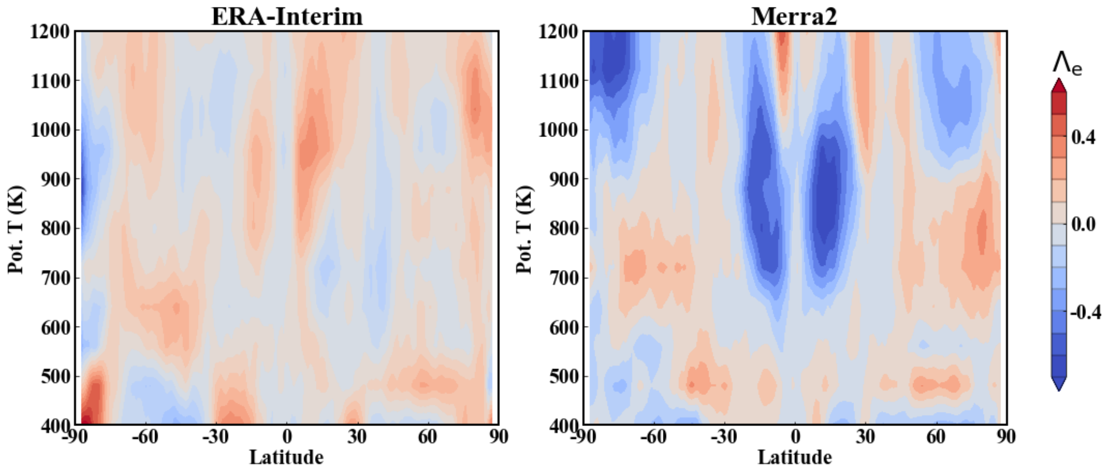

Figure 6. Distribution of long-term linear trends ($a(\phi,z)$) in multiple regression results for ERA-Interim and MERRA-2 data.

The atmospheric variability signals of QBO and ENSO and the complex interactions between them affect interannual variability of the isentropic mixing intensity. Therefore, to clarify the influences of QBO and ENSO on stratospheric wave breaking, the regression fitting is projected onto the basis functions of QBO and ENSO to represent QBO and ENSO signals ($\Delta 1 = b1 \times p1$; $\Delta 2 = b2 \times p2$), where p1 is the QBO index, the normalized 50 hPa zonal mean wind speed, and p2 is the normalized multivariate ENSO index (MEI).

Figures 7 and 8 show the QBO and ENSO signals in the isentropic mixing during 1980–2010, respectively. In Figure 7, it is clear that the mixing in the lower stratosphere is suppressed in the equatorial region and enhanced in the subtropical and mid-latitude regions under the WQBO phase, while the two datasets show opposite results in the polar region of the Northern Hemisphere. The criterion we use to divide the easterly and westerly phases is the zonal average wind at 50 hPa, which is not consistent with the zonal wind at 480 K (about 60 hPa). Thereby, the results under the westerly phase do not satisfy the Holton–Tan effect. The results at 880 K in the middle stratosphere are opposite to the results in the lower level, and the mixing is stronger in the middle and lower latitudes in the easterly phase. The two datasets are consistent, indicating that more planetary waves are reflected to the middle latitudes in the middle and upper stratosphere under the EQBO phase, and thus, the perturbation is also stronger in this region, which is consistent with the Holton–Tan effect.

Figure 8 shows that there is little difference in the ENSO signal in the lower stratosphere between the two datasets. The mixing in the high latitudes is weak in the El Niño years, and the opposite is true in the high latitudes in the La Niña years. The two datasets in the mid-stratosphere are consistent in the mid-latitudes and polar regions, and the mixing in the El Niño years is stronger in the mid-latitudes and weaker in the polar region. In the El Niño years, the upward propagation of the planetary waves strengthens, and the wave breaking occurs in the mid-latitudes, resulting in a weaker than normal polar vortex in the Northern Hemisphere. As a result, the waves become stronger in the mid-latitudes and weaker in the polar region. In the middle stratosphere over the tropics, the two datasets are quite different. ERA-Interim shows that the mixing is enhanced in the equatorial region in the El Niño years, while the MERRA2 data show that the mixing is weakened. A previous study found that the subtropical jet shifts toward the equator and moves upward in the El Niño years, resulting in enhanced wave breaking in this region, and the mixing in the tropics is enhanced subsequently [50]. Results of this study are consistent with what we found based on ERA-Interim.

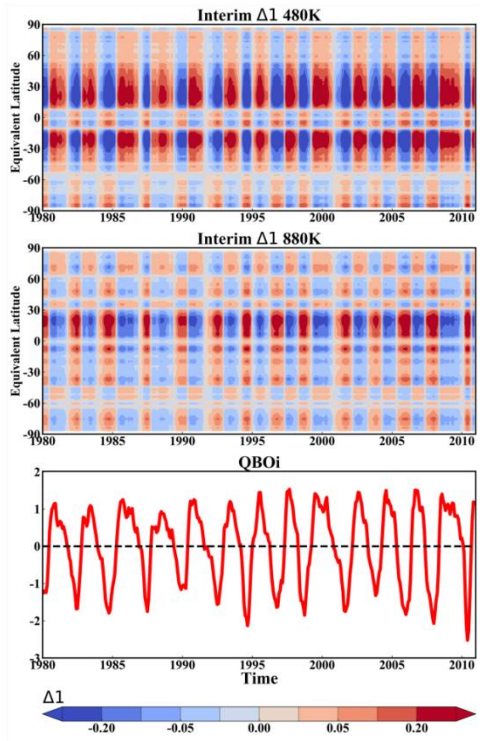

Figure 7. Time-latitude cross-sections at 480 K and 880 K based on ERA-Interim (**left**) and MERRA2 (**right**) from 1980 to 2010 for calculation using the basis function in the multiple regression model ($\Delta1 = b1 \times p1$).

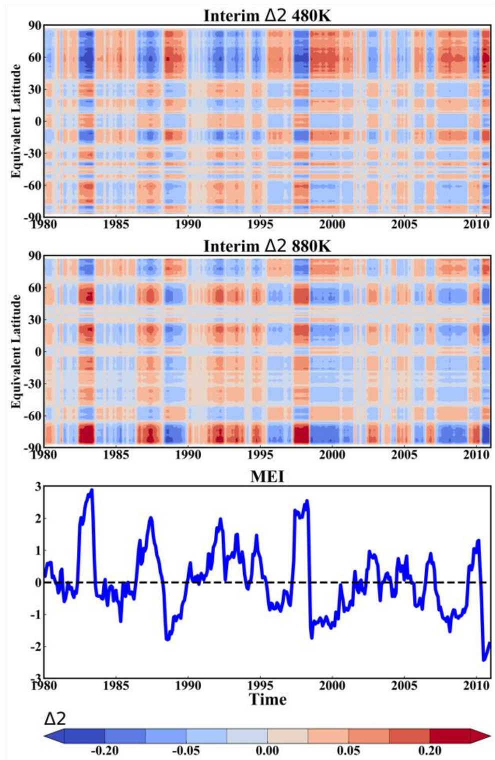

Figure 8. Time-latitude cross-sections at 480 K and 880 K based on ERA-Interim (**left**) and MERRA2 (**right**) from 1980 to 2010 for calculation using the basis function in the multiple regression model ($\Delta2 = b2 \times p2$).

3.3. Composite Analysis of Modulation of Stratospheric Mixing by QBO and ENSO

Figure 9 displays composite latitude-height cross-sections of zonal mean equivalent length, the zonal wind, vertical and horizontal components of E–P fluxes, and E–P flux divergence anomalies (see Section 2 for the calculation method) in the Northern and Southern Hemispheres in winter in the WQBO and EQBO phases based on the ERA-Interim reanalysis product. Changes in speed and direction of stratospheric zonal wind induced by QBO can affect the path of the wave propagation, and the anomalies of the zonal wind in the WQBO and EQBO phases correspond to the distributions of the equivalent length in the two QBO phases. At around 30°N, wind speed tends to decrease, and uploaded planetary waves are converged in the region, thus leading the planetary waves in the stratosphere to increase, and mixing is enhanced during the WQBO phase. In the EQBO phase, however, the mixing in this area is suppressed. The above results are consistent with the results of Shuckburgh et al. [30]. In the WQBO phase, the wind speed is stronger near 60°N upward propagation of planetary wave divergence, which is not conducive to planetary wave breaking, and the mixing in this area is weak. The opposite is true in the EQBO phase when the wind speed near 60°N is weak and more planetary waves converge. As a result, wave disturbances are stronger near 60°N, and the mixing enhances, which is consistent with the Holton–Tan effect. In the Southern Hemisphere winter, the mixing in the mid-latitudes is relatively weak under the WQBO phase, while more planetary waves are reflected to the mid- and high latitudes in the EQBO phase, and the mixing is also significantly strong. Compared with that in the Northern Hemisphere, the Holton–Tan effect is more significant in the Southern Hemisphere.

Figure 10 presents composite latitude-height cross-sections of zonal mean equivalent lengths in the El Niño and La Niña years and corresponding anomalies of the E–P flux and zonal wind anomalies based on ERA-Interim reanalysis data in the Northern and Southern Hemispheres. Several previous studies have shown that the propagation of Rossby waves to the stratosphere enhances during the El Niño years in the Northern Hemisphere, resulting in stronger mixing in the mid- and high latitudes [31,51]. However, in the present study, due to the different criteria used for identifying the El Niño and La Niña events, the analysis results show that the ENSO impact on the intensity of isentropic mixing in the stratosphere is closely related to the position of the polar jet and changes in zonal wind speed, presenting a more complicated pattern. In the winter of the El Niño years, the polar jet in the Northern Hemisphere moves northward, which leads to more wave activities near 30°N, and the mixing also increases. The increased wind speed planetary wave divergence in the middle and high latitudes suppresses the wave breaking, and the mixing weakens correspondingly during the El Niño years. In the La Niña years, wind speed weakens, and more planetary waves converge so that wave activities increase in the mid-latitudes. In the La Niña years, the polar jet in the Southern Hemisphere moves northward, and the wind speed becomes stronger near 30°S, which is not conducive to wave breaking. The mixing weakens around 30°S but enhances near 60°S. In the El Niño years, the mixing is weak in places where the wind speed is strong. Note that weak wind speed is conducive to the breaking of planetary waves, and thus, the mixing is strong in places of weak wind speed.

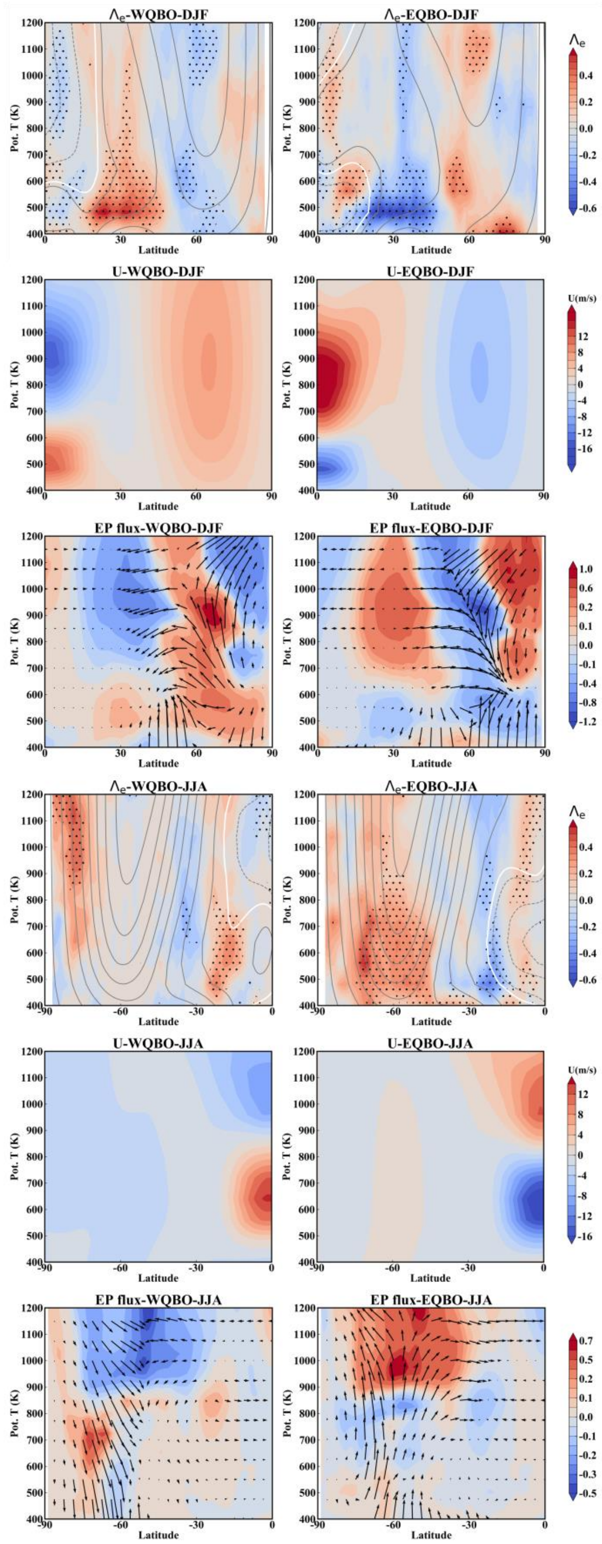

Figure 9. Composite latitude-height cross-sections of zonal mean equivalent length and E–P flux (vectors) and E–P flux divergence (color shadings) in the Northern and Southern Hemispheres in winter in the WQBO and EQBO phases based on the ERA-Interim reanalysis product and corresponding zonal wind anomalies. Black dotted areas are for values significant at the 90% confidence level by *t*-test. Cases used for composite analysis are listed in Table 1. The contours show zonal mean wind at 10 m/s intervals (solid gray lines are for westerly winds, dashed gray lines are for easterly winds, and the white lines indicate zero wind speed).

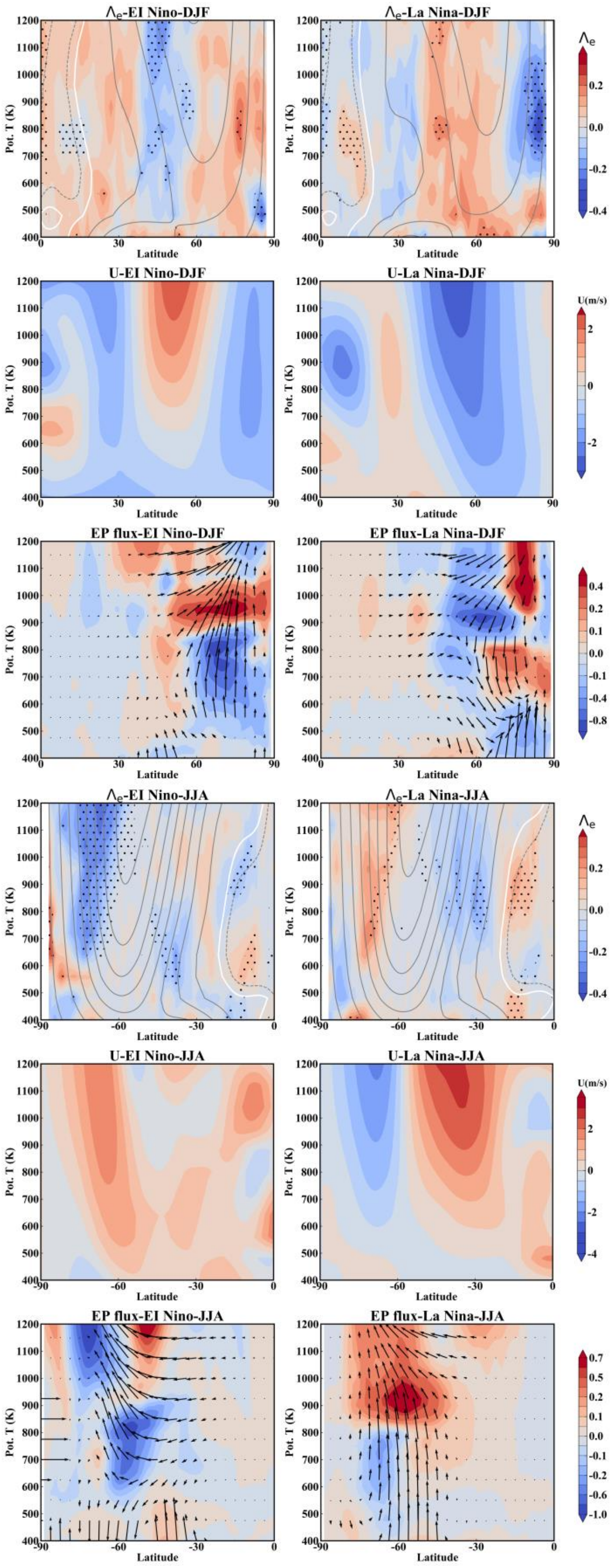

Figure 10. Composite latitude-height cross-sections of zonal mean equivalent lengths and E–P flux (vectors) and E–P flux divergence (color shadings) in the El Niño and La Niña years and corresponding zonal wind anomalies based on ERA-Interim reanalysis data for the period 1980–2010. The black dotted area represents values passing the 90% confidence level test (by *t*-test). The cases used for composite analysis are shown in Table 2. The contours show mean zonal winds at intervals of 10 m/s (solid gray lines for westerly winds, dashed gray lines for easterly winds, and white lines for zero winds).

4. Summary and Discussion

Based on the potential vorticity data extracted from the ERA-Interim and MERRA-2 reanalysis products, the influences of the quasi-biennial oscillation and the El Niño–Southern Oscillation on the intensity of isentropic mixing in the stratosphere are analyzed using multiple regression and composite analysis methods. Obvious QBO signals can be found in the tropics. In winter, there is an area of strong mixing with clear boundary in the middle latitudes of the stratosphere, which corresponds to the surf zone where the mixing is strong and the QBO signal is obvious. The fitting of the multiple regression model is less ideal than expected in the equatorial region, but the model can well fit the temporal evolution of the equivalent length in the mid-latitudes and polar region.

Analysis of the basis function of QBO in the multiple regression model shows that the mixing in the lower stratosphere in the WQBO phase is suppressed in the equatorial region, but the mixing in the subtropical and mid-latitude regions enhances. The results in the westerly phase are not consistent with the Holton–Tan effect. In the middle stratosphere, more planetary waves are reflected to the mid-latitude region in the EQBO phase, and thus the disturbance in this region also becomes stronger, which is consistent with the Holton–Tan mechanism. Respective composite analyses of cases in the WQBO and EQBO phases reveal that QBO-induced changes in the direction and speed of zonal wind in the stratosphere can affect wave propagation speed and path. In the WQBO phase, wind speed weakens near 30°N in the Northern Hemisphere, but the mixing enhances in this area. However, the mixing in this area is suppressed in the EQBO phase. In the EQBO phase, the wind speed near 60°N is relatively weak and more planetary waves breaking are found in the region. The mixing in this region is weak in the WQBO phase. These results around 60°N are consistent with the Holton–Tan effect. Compared with that in the Northern Hemisphere, the Holton–Tan effect is more significant in the Southern Hemisphere.

Multiple regression analysis shows the ENSO influence on the intensity of isentropic mixing, which is manifested in the El Niño years with weaker mixing at middle and high latitudes and stronger mixing at low latitudes in the lower stratosphere. In the middle stratosphere, upward propagation of planetary waves enhances and isentropic mixing intensifies in the mild latitudes but weakens in polar region. Results from the two reanalysis products are opposite in the low latitudes. In the El Niño years, ERA-Interim indicates that the isentropic mixing intensifies, whereas MERRA2 indicates the mixing weakens. In the La Niña years, changes in isentropic mixing are opposite to that in the El Niño years. Composite analysis reveals that the areas of strong and weak mixing in the El Niño and La Niña years are significantly related to changes in the location and wind speed of the polar jet. In the Northern Hemisphere winter, the polar jet moves northward in the El Niño years, and the mixing enhances near 30°N; meanwhile, wind speed increases and planetary wave divergence enhances near 60°N, suppressing wave breaking and weakening the mixing there. In the La Niña years, wind speed decreases in the mid-latitudes, and the mixing intensifies. In the Southern Hemisphere winter, ENSO also modulates the strength of the zonal wind and consequently affects the strength of isentropic mixing. The mixing is weak in places where the wind is strong. Weak wind is conducive to the breaking of nearly stationary planetary waves, and thus, the mixing is strong in places of weak wind speed.

Author Contributions: Conceptualization, J.L. (Jing Liang); methodology, J.L. (Jing Liang) and Z.W.; software, J.L. (Jing Liang); validation, Z.W. and J.L. (Jiali Luo); formal analysis, J.L. (Jing Liang); investigation, J.L. (Jing Liang); resources, Z.W.; data curation, J.L. (Jing Liang) and Z.Z.; writing—original draft preparation, J.L. (Jing Liang); writing—review and editing, J.L. (Jing Liang) and Z.W.; visualization, J.L. (Jing Liang) and Z.Z.; supervision, Z.W. and J.L. (Jiali Luo); project administration, Z.W.; funding acquisition, Z.W. All authors have read and agreed to the published version of the manuscript.

Funding: This research was funded by the National Natural Science Foundation of China General Projects (grant number 42275072) and the National Natural Science Foundation of China Project (grant number 41805030).

Data Availability Statement: Data openly available in a public repository. The data analyzed in this study were extracted from the following web addresses: ERA-interim data: https://www.ecmwf.int/en/forecasts/dataset/ecmwf-reanalysis-interim (accessed on 1 March 2023); MERRA2 data: https://disc.gsfc.nasa.gov/datasets/M2IMNPASM_5.12.4/ (accessed on 1 March 2023).

Acknowledgments: This research is funded by NSFC General Projects 42275072 and the NSFC Project 41805030.

Conflicts of Interest: The authors declare no conflict of interest.

References

1. Alan, P.R. Stratospheric Transport. *J. Meteorol. Soc. Jpn. Ser. II* **2002**, *80*, 793–809.
2. Shepherd, T.G. Transport in the Middle Atmosphere. *J. Meteorol. Soc. Jpn. Ser. II* **2007**, *85*, 165–191. [CrossRef]
3. Mcintyre, M.E.; Palmer, T.N. The 'surf zone' in the stratosphere. *J. Atmos. Terr. Phys.* **1984**, *46*, 825–849. [CrossRef]
4. Nakamura, N. Two-dimensional mixing, edge formation, and permeability diagnosed in an area coordinate. *J. Atmos.* **1996**, *53*, 1524–1537. [CrossRef]
5. Nakamura, N.; Ma, J. Modified Lagrangian-mean diagnostics of the stratospheric polar vortices: 2. Nitrous oxide and seasonal barrier migration in the cryogenic limb array etalon spectrometer and SKYHI general circulation model. *J. Geophys. Res. Atmos.* **1997**, *102*, 25721–25735. [CrossRef]
6. Haynes, P.; Shuckburgh, E. Effective Diffusivity as a diagnostic of atmospheric transport. Part 1: Stratosphere. *J. Geophys. Res. Atmos.* **2000**, *105*, 22777–22794. [CrossRef]
7. Haynes, P.; Shuckburgh, E. Effective diffusivity as a diagnostic of atmospheric transport: 2. Troposphere and lower stratosphere. *J. Geophys. Res.* **2000**, *105*, 22795. [CrossRef]
8. Mcintyre, M.E.; Palmer, T. Breaking waves in the stratosphere. *Nature* **1983**, *305*, 593–600. [CrossRef]
9. Chen, P. The Influences of Zonal Flow on Wave Breaking and Tropical-Extratropical Interaction in the Lower Stratosphere. *J. Atmos. Sci.* **1996**, *53*, 2379–2392. [CrossRef]
10. O'Sullivan, D.; Ping, C. Modeling the quasi biennial oscillation's influence on isentropic tracer transport in the subtropics. *J. Geophys. Res. Atmos.* **1996**, *101*, 6811–6821. [CrossRef]
11. Manzini, E.; Giorgetta, M.A.; Esch, M.; Kornblueh, L.; Roeckner, E. The Influence of Sea Surface Temperatures on the Northern Winter Stratosphere: Ensemble Simulations with the MAECHAM5 Model. *J. Clim.* **2006**, *19*, 3863–3881. [CrossRef]
12. Camp, C.D.; Tung, K.K. Stratospheric polar warming by ENSO in winter: A statistical study. *Geophys. Res. Lett.* **2007**, *34*, 545–559. [CrossRef]
13. Zhang, J.; Tian, W.; Wang, Z.; Xie, F.; Wang, F. The Influence of ENSO on Northern Midlatitude ozone during the Winter to Spring Transition. *J. Clim.* **2015**, *28*, 4774–4793. [CrossRef]
14. Xie, F.; Li, J.; Tian, W.; Fu, Q.; Jin, F.F.; Hu, Y.; Zhang, J.; Wang, W.; Sun, C.; Feng, J.; et al. A connection from Arctic stratospheric ozone to El Nio-Southern oscillation. *Environ. Res. Lett.* **2016**, *11*, 124026. [CrossRef]
15. Ruzmaikin, A.; Feynman, J.; Jiang, X.; Fu, Q.; Jin, F.-F.; Hu, Y.; Zhang, J.; Wang, W.; Sun, C.; Feng, J.; et al. Extratropical signature of the quasi-biennial oscillation. *J. Geophys. Res. Atmos.* **2005**, *110*, 124026. [CrossRef]
16. Garfinkel, C.I.; Shaw, T.A.; Hartmann, D.L.; Waugh, D.W. Does the Holton–Tan Mechanism Explain How the Quasi-Biennial Oscillation Modulates the Arctic Polar Vortex? *J. Atmos. Sci.* **2012**, *69*, 1713–1733. [CrossRef]
17. Wen, C.; Takahashi, M.; Graf, H.F. Interannual variations of stationary planetary wave activity in the northern winter troposphere and stratosphere and their relations to NAM and SST. *J. Geophys. Res. Atmos.* **2003**, *108*, 4797. [CrossRef]
18. And, C.; Hartmann, D.L. Effects of the El Niño–Southern Oscillation and the Quasi-Biennial Oscillation on polar temperatures in the stratosphere. *J. Geophys. Res. Atmos.* **2007**, *D19112*. [CrossRef]
19. Ineson, S.; Scaife, A.A. The role of the stratosphere in the European climate response to El Niño. *Nat. Geosci.* **2009**, *2*, 32–36. [CrossRef]
20. Holton, J.R.; Tan, H.C. The Influence of the Equatorial Quasi-Biennial Oscillation on the Global Circulation at 50 mb. *J. Atmos.* **1980**, *37*, 2200–2208. [CrossRef]
21. Plumb, R.A.; Bell, R.C. A model of the quasi-biennial oscillation on an equatorial beta-plane. *Q. J. R. Meteorol. Soc.* **1982**, *108*, 335–352. [CrossRef]
22. White, I.P.; Lu, H.; Mitchell, N.J. Seasonal evolution of the QBO-induced wave forcing and circulation anomalies in the northern winter stratosphere. *J. Geophys. Res. Atmos.* **2018**, *121*, 410–411. [CrossRef]
23. Silverman, V.; Lubis, S.W.; Harnik, N.; Matthes, K. A Synoptic View of the Onset of the Midlatitude QBO Signal. *J. Atmos. Sci.* **2021**, *78*, 3759–3780.
24. Sassi, F. Effect of El Nino–Southern Oscillation on the dynamical, thermal, and chemical structure of the middle atmosphere. *J. Geophys. Res.* **2004**, *109*, D17108. [CrossRef]
25. García-Herrera, R.; Calvo, N.; Garcia, R.R.; Giorgetta, M.A. Propagation of ENSO temperature signals into the middle atmosphere: A comparison of two general circulation models and ERA-40 reanalysis data. *J. Geophys. Res. Atmos.* **2006**, *D06101*. [CrossRef]
26. Thompson, E.P.L.H. Seasonal Evolution of Stratosphere-Troposphere Coupling in the Southern Hemisphere and Implications for the Predictability of Surface Climate. *J. Geophys. Res. D Atmos. JGR* **2018**, *123*, 12002–12016.

27. Loon, H.V.; Zerefos, C.S.; Repapis, C.C. The Southern Oscillation in the Stratosphere. *Mon. Weather Rev.* **1982**, *110*, 225–229. [CrossRef]
28. Loon, H.V.; Labitzke, K. The Southern Oscillation. Part V: The Anomalies in the Lower Stratosphere of the Northern Hemisphere in Winter and a Comparison with the Quasi-Biennial Oscillation. *Mon. Weather Rev.* **1987**, *115*, 559–565.
29. Hamilton, K. An examination of observed Southern Oscillation effects in the Northern Hemisphere stratosphere. *J. Atmos.* **1993**, *50*, 3468–3474. [CrossRef]
30. Shuckburgh, E.; Norton, W.; Iwi, A.; Haynes, P. Influence of the quasi-biennial oscillation on isentropic transport and mixing in the tropics and subtropics. *J. Geophys. Res. Atmos.* **2001**, *106*, 14327–14337. [CrossRef]
31. Garny, H.; Bodeker, G.; Dameris, M. Trends and variability in stratospheric mixing: 1979–2005. *Atmos. Chem. Phys.* **2007**, *7*, 5611–5624. [CrossRef]
32. Chen, G.; Lu, J.; Frierson, D.M.W. Phase Speed Spectra and the Latitude of Surface Westerlies: Interannual Variability and Global Warming Trend. *J. Clim.* **2008**, *21*, 5942–5959. [CrossRef]
33. Shuckburgh, E.; D Ovidio, F.; Legras, B. Local Mixing Events in the Upper Troposphere and Lower Stratosphere. Part II: Seasonal and Interannual Variability. *J. Atmos. Sci.* **2009**, *66*, 3695–3706. [CrossRef]
34. Yang, H.; Chen, G.; Domeisen, D.I.V. Sensitivities of the Lower-Stratospheric Transport and Mixing to Tropical SST Heating. *J. Atmos. Sci.* **2014**, *71*, 2674–2694. [CrossRef]
35. Abalos, M.; Legras, B.; Shuckburgh, E. Interannual variability in effective diffusivity in the upper troposphere/lower stratosphere from reanalysis data. *Q. J. R. Meteorol. Soc.* **2016**, *142*, 1847–1861. [CrossRef]
36. Hoskins, B.J.; Mcintyre, M.E.; Robertson, A.W. On the use and significance of isentropic potential vorticity maps. *Q. J. R. Meteorol. Soc.* **1985**, *111*, 877–946. [CrossRef]
37. Bodeker, G.E.; Scott, J.C.; Kreher, K.; McKenzie, R.L. Global ozone trends in potential vorticity coordinates using TOMS and GOME intercompared against the Dobson network: 1978–1998. *J. Geophys. Res.* **2001**, *106*, 23029. [CrossRef]
38. Waugh, D.W.; Rong, P.P. Interannual Variability in the Decay of Lower Stratospheric Arctic Vortices. *J. Meteorol. Soc. Jpn.* **2002**, *80*, 997–1012. [CrossRef]
39. Abalos, M.; Randel, W.J.; Birner, T. Phase-speed Spectra of Eddy Tracer Fluxes Linked to Isentropic Stirring and Mixing in the Upper Troposphere and Lower Stratosphere. *J. Atmos. Sci.* **2016**, *73*, 4711–4730. [CrossRef]
40. Diallo, M.; Legras, B.; Chédin, A. Age of stratospheric air in the ERA-Interim. *Atmos. Chem. Phys.* **2012**, *12*, 17087–17134. [CrossRef]
41. Diallo, M.; Ploeger, F.; Konopka, P.; Birner, T.; Müller, R.; Riese, M.; Riese, M.; Garny, H.; Legras, B.; Ray, E.; et al. Significant Contributions of Volcanic Aerosols to Decadal Changes in the Stratospheric Circulation. *Geophys. Res. Lett.* **2017**, *44*, 710–780. [CrossRef]
42. Diallo, M.; Riese, M.; Birner, T.; Konopka, P.; Müller, R.; Hegglin, M.I.; Santee, M.L.; Baldwin, M.; Legras, B.; Ploeger, F. Response of stratospheric water vapor and ozone to the unusual timing of El Niño and the QBO disruption in 2015–2016. *Atmos. Chem. Phys.* **2018**, *18*, 13055–13073. [CrossRef]
43. Wolter, K.; Timlin, M.S. El Niño/Southern Oscillation behaviour since 1871 as diagnosed in an extended multivariate ENSO index (MEI.ext). *Int. J. Clim.* **2011**, *31*, 1074–1087. [CrossRef]
44. Andrews, D.G.; Holton, J.R.; Leovy, C.B. *Middle Atmosphere Dynamics*; Academic Press: San Diego, CA, USA, 1987.
45. Edmon, H.J., Jr.; Hoskins, B.J.; McIntyre, M.E. Eliassen-palm cross sections for the troposphere. *J. Atmos. Sci.* **1980**, *37*, 2600–2616. [CrossRef]
46. Kiem, A.S.; Franks, S.W. On the identification of ENSO-induced rainfall and runoff variability: A comparison of methods and indices. *Int. Assoc. Sci. Hydrol. Bull.* **2001**, *46*, 715–727. [CrossRef]
47. Lu, A.; Zhu, W.; Jia, S. Assessment of the sensitivity of vegetation to El-Nino/Southern Oscillation events over China. *Adv. Space Res.* **2012**, *50*, 1362–1373. [CrossRef]
48. Bastos, A.; Running, S.W.; Gouveia, C.; Trigo, R.M. The global NPP dependence on ENSO: La Nina and the extraordinary year of 2011. *J. Geophys. Res. Biogeosci.* **2013**, *118*, 1247–1255. [CrossRef]
49. Wen, C.; Lei, Y.; Ronghui, H.; Qihong, Q. Diagnostic Analysis of the Impact of Tropical QBO on the General Circulation in the Northern Hemisphere Winter. *Chin. J. Atmos. Sci.* **2004**, *28*, 161–173.
50. Domeisen, D.; Garfinkel, C.I.; Butler, A.H. The Teleconnection of El Niño Southern Oscillation to the Stratosphere. *Rev. Geophys.* **2019**, *57*, 5–47. [CrossRef]
51. Calvo, N.; Garcia, R.R.; Randel, W.J.; Marsh, D. Dynamical Mechanism for the Increase in Tropical Upwelling in the Lowermost Tropical Stratosphere during Warm ENSO Events. *J. Atmos. Sci.* **2009**, *67*, 2331–2340. [CrossRef]